Springer

KSME

Journal of Mechanical Science and Technology 33 (6) (2019) 2511~2525
www.springerlink.com/content/1738-494x(Print)/1976-3824(Online)
DOI 10.1007/s12206-019-0501-0

Effect of the raceway defects on the nonlinear dynamic behavior of rolling bearing †

Ziqiang Zhao, Xuebin Yin and Wenzhong Wang*

School of Mechanical Engineering, Beijing Institute of Technology, Beijing 100081, China

(Manuscript Received February 14, 2018; Revised January 31, 2019; Accepted March 9, 2019)

Abstract

The defects on raceways would aggravate the vibration of bearing and greatly influence the bearing performance, in order to monitor the running state of the bearing and detect the early defect, the characteristics induced by the defect must be explored. This paper establishes a bearing dynamic model to explore the effect of raceway defects on the nonlinear dynamic behavior of rolling element bearing. The interaction between ball and races is modeled based on Hertz theory, while the presence of defects changes the ball-race interaction. The effects of defect size, position and number on bearing dynamic behaviors are investigated with the aid of phase trajectories, shaft center orbits, FFT spectra, etc. The results indicate that the defects can make the motion of the system more complicated and induce vibration at some characteristic frequencies, which can be used to recognize the bearing failure at early stage. The proposed research provides useful information for the design and status monitoring of mechanical systems.

Keywords: Rolling bearing; Raceway defects; Dynamic behavior; Characteristic frequency; Phase trajectories

1. Introduction

Since rolling element bearing serves as one of the most important supporting parts of transmission system, dynamic characteristics of rolling bearing have significant effects on the performance of mechanical equipment. With the development of modern industry and scientific technology, equipment has higher requirements on the load capacity, dynamic performance, reliability and precision of rolling bearing. However, in the manufacturing and service process, various defects may arise on the surface of raceways, which could induce increasing vibration. Defects located on the races, such as, pits, cracks and spalls, work as an internal excitation, will affect the bearing dynamics performance.

A lot of researches have been conducted to understand the effect of various defects on the bearing behaviors. Tandon and Choudhury [1] summarized the methods for vibration and acoustic measurement in detecting both localized and distributed defects in bearing. However, only few researches established mathematical model for rolling bearing with localized defects. McFadden and Smith [2, 3] presented the mechanical model of rolling bearing with defects. At first, rolling bearing with one single defect on inner raceway under constant radial load was researched. Then the model was extended to two defects. A series of pulse string had also been used to stand for the vibration response of ball passing defects, and the validation of the model is verified by their experiments. Tandon and Choudhury [4] developed an analytical model to investigate the vibration frequencies of rolling element bearing caused by a single local defect under both radial and axial loads. They used the pulses with different widths to represent the vibration response caused by defect; the shapes of pulses include rectangular, triangular and half-sine pulse. It was found that the vibration amplitude induced by the outer race defect is much high in comparison to the defect on inner raceway and rolling element. Sopanen and Mikola [5, 6] developed a six-degree of freedom dynamic model for deep groove ball bearing to investigate the effect of both local and distributed defects with consideration of elastohydrodynamic lubrication. It was found that radial clearance greatly influences the vibration response and natural frequencies of the bearing system. Kıral and Karagülle [7] conducted finite element analysis to investigate the vibration of rolling element bearings with localized defects under unbalanced force. Ashtekar et al. [8] developed a dynamic model for both deep groove and angular contact ball bearing with dents on inner and outer raceways, cage and balls using their own modified Hertzian force-deflection relationship function. Rafsanjani et al. [9] proposed an analytical model considering the internal radial clearance and solved based on a modified Newmark time integration technique and the classical Floquet theory. Patil et al. [10] proposed a theoretical model to predict the vibration of rolling element bearing with a circumferential half sinusoidal wave defect. In this model, the contact between ball and races is considered as nonlinear spring, the contact force is obtained by Hertz contact

*Corresponding author. Tel.: +86 1068911404, Fax.: +86 1068911404
E-mail address: wangwzhong@bit.edu.cn
† Recommended by Associate Editor Jin Woo Lee

theory. Nakhaeinejad and Bryant [11] proposed a dynamic model of faulty rolling element bearing utilizing vector bond graphs in which the surface profile changes represent the defects on raceways. Kulkarni and Sahasrabudhe [12] developed a dynamic model of ball bearing using cubic Hermite spline to simulate the process when the ball strikes the defects on outer race. Recent work done by Govardhan et al. [13] investigated the excitations caused by bearing defect under dynamic radial load which was considered to be composed of a static and a harmonic components. Liu et al. [14] investigated the effect of the defect depth on bearing vibration considering the time-varying displacement and contact stiffness for the first time. Moreover, Sassi [15], Arslan [16], and Patel [17] also had done some works on the vibration of bearing with surface defects. In these researches, bearing with single and multiple defects were investigated, and the characteristic frequencies can be found in the spectrums. Besides the localized and distributed defects above, some researchers also paid attention to the vibration induced by the bearing material defects, e.g. material inclusions [18], which would also make the motion of the system more complicated.

It can be found that most studies focus on the waviness [19-22] or the defect on raceways. For localized defects, only a few researchers have investigated the effect of one or two defects on inner or outer race by means of numerical method. However, it is inevitable to produce even more defects on races, and the distribution of defects may be uniform or random. Moreover, surface defects coupled interface friction or the eccentricity of the bearing-rotor system is barely investigated until now.

In this paper, a model has been established to systematically investigate the influence of size of defect, number of defects, defect location, distribution of defects, and defect coupled interface friction or the eccentricity of the bearing-rotor system. In the present model, the contact force between balls and raceways is calculated based on the Hertz contact theory. The kinematic relationship between balls and races is established with raceway control hypothesis. The contact deformation is figured out considering the defect. The set of nonlinear differential equations of motion is solved based on the fourth order Runge-Kutta method. After the proposed model is validated by the existent model, the effect of size, number, and distribution of defect, etc is explored finally.

2. Theoretical model

2.1 Dynamic model of deep groove ball bearing

In order to establish the kinematic equations, following hypotheses are made:

(1) "Rigid ring hypothesis" is adopted, namely, only the local elastic contact deformation between balls and raceways is considered, and the elastic-plastic deformation of the whole bearing rings is ignored.

(2) The balls are in pure rolling on the bearing raceways.

For deep groove ball bearing, the orbital angular velocity of steel balls is

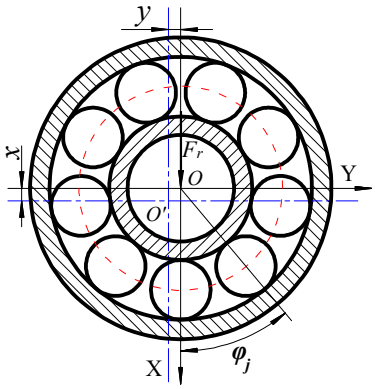

Fig. 1. The schematic diagram of deep groove ball bearing.

$$\omega_c = \omega_i \cdot \frac{D_i}{D_i + D_e} \tag{1}$$

where ω_i is the angular velocity of inner ring, D_i and D_e are the groove bottom diameters of inner raceway and outer raceway, respectively.

Without loss of generality, it is assumed that the outer ring of the bearing is rigid and fixed. As shown in Fig. 1, due to the radial force F_r, the center of inner ring has the displacements in both x and y directions. At any instant t, the displacement of inner race groove bottom at the azimuth angle φ_j can be written as

$$d_j = x\cos\varphi_j + y\sin\varphi_j \tag{2}$$

where φ_j is the azimuth angle of jth ball. Assuming that the bearing has a total of Z balls, φ_j can be written as

$$\varphi_j = 2\pi(j-1)/Z + \omega_c \cdot t. \tag{3}$$

Assume that the radial clearance of the bearing is u; then the elastic deformation between the jth ball and raceways at the azimuth angle φ_j is

$$\delta_j = d_j - u. \tag{4}$$

Based on the Hertz contact theory, the contact force Q_j between the jth ball and the races can be obtained as follows:

$$Q_j = \begin{cases} K\delta_j^{1.5} & \forall \delta_j \geq 0 \\ 0 & \forall \delta_j < 0 \end{cases} \tag{5}$$

where K is the load-displacement coefficient which can be obtained from the following formula [23]:

$$K = \left[\frac{1}{(1+K_i)^{1/n} + (1+K_e)^{1/n}} \right]^n. \tag{6}$$

For point contact, the index n is 1.5 and 1.11 for the line contact. K_i and K_e are the load-displacement coefficients for the contacts between ball and inner raceway or outer raceway, respectively, which are evaluated by following equations

$$K_i = \frac{4\sqrt{2}E'}{3(\sum\rho_i)^{1/2}}\left(\frac{1}{\delta_i^*}\right)^n \tag{7}$$

$$K_e = \frac{4\sqrt{2}E'}{3(\sum\rho_e)^{1/2}}\left(\frac{1}{\delta_e^*}\right)^n \tag{8}$$

where $\sum\rho$ is the curvature sum of the contact point, E' is the equivalent elastic modulus which can be calculated as follows:

$$\frac{1}{E'} = \frac{1-\nu_1^2}{E_1} + \frac{1-\nu_2^2}{E_2} \tag{9}$$

where E_1, E_2 are the Young's modulus, and v_1 v_2 are the Poisson's ratio, respectively. δ* in Eqs. (7) and (8) is the dimensionless contact coefficient which can be evaluated by following formula:

$$\delta^* = \frac{2L_1(\kappa)}{\pi}\left(\frac{\pi}{2\kappa^2 L_2(\kappa)}\right)^{1/3} \tag{10}$$

where $L_1(\kappa)$, $L_2(\kappa)$ are the first and second kind of complete elliptic integrals with κ is the ellipticity of the contact area, they are calculated by the following equations:

$$\begin{cases} L_1(\kappa) = \int_0^{\pi/2}\left[1-\left(1-\frac{1}{\kappa^2}\right)\sin^2\theta\right]^{-1/2} d\theta \\ L_2(\kappa) = \int_0^{\pi/2}\left[1-\left(1-\frac{1}{\kappa^2}\right)\sin^2\theta\right]^{1/2} d\theta\,. \end{cases} \tag{11}$$

The contact forces applied on inner race by all the balls can be divided into the components in x and y directions and expressed as

$$\begin{bmatrix} Q_x \\ Q_y \end{bmatrix} = \sum_{j=1}^{Z} Q_j \begin{bmatrix} \cos\varphi_j \\ \sin\varphi_j \end{bmatrix}. \tag{12}$$

Finally, the differential equations of motion for the bearing-rotor system can be established as follows,

$$\begin{cases} M\ddot{x} + C\dot{x} + Q_x = F_r + Me\omega_i^2\cos\omega_i t \\ M\ddot{y} + C\dot{y} + Q_y = Me\omega_i^2\sin\omega_i t \end{cases} \tag{13}$$

where M is the total mass of shaft and inner ring, C is the damping coefficient, e is the eccentricity of the unbalanced mass of the bearing-rotor system. If the system is well balanced, the eccentricity $e = 0$.

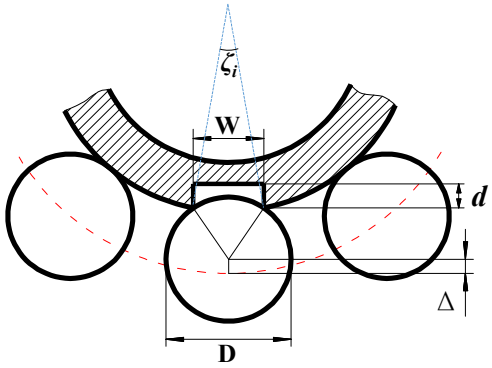

(a) Defect on inner raceway

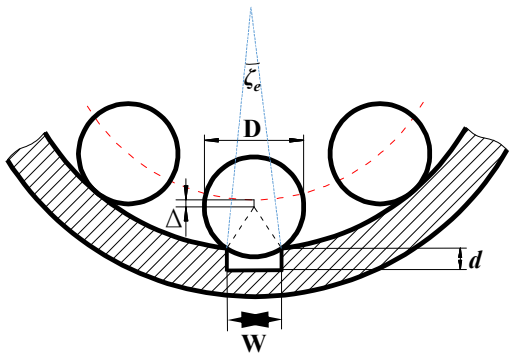

(b) Defect on outer raceway

Fig. 2. Schematic diagram of defect on inner raceway and outer raceway.

Eq. (13) is the second order nonlinear differential equation, which can be rewritten as the following set of the first order differential equations:

$$\begin{cases} \dot{z}_1 = z_2 \\ \dot{z}_2 = \frac{F_r + Me\omega_i^2\cos\omega_i t}{M} - \frac{C}{M}z_2 - \frac{Q_x}{M} \\ \dot{z}_3 = z_4 \\ \dot{z}_4 = \frac{Me\omega_i^2\sin\omega_i t}{M} - \frac{C}{M}z_4 - \frac{Q_y}{M} \end{cases} \tag{14}$$

where $z_1 = x$, $z_2 = \dot{x}$, $z_3 = y$, $z_4 = \dot{y}$.

2.2 Surface defect model

Figs. 2(a) and (b) schematically show the defect appeared on outer raceway and inner raceway, respectively. When the ball rolls over the defect, the additional displacement Δ of the ball center can be obtained as follows,

$$\Delta = \frac{D}{2}\left(1-\cos\frac{W}{D}\right) \tag{15}$$

where W is the width of the defect, D is the ball diameter. Since the width of the defect is much smaller relative to the ball diameter, the additional displacement Δ is tiny when the

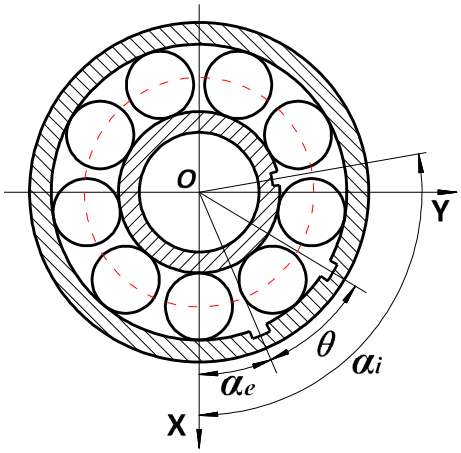

Fig. 3. Schematic diagram of bearing with surface defects.

ball is riding over the defect. It can be assumed that the depth d of the defect is greater than the additional displacement Δ, then the influence of the depth of the defect is not taken into account. Here, the rectangular defect is assumed as an example, the defect with other shapes can be considered through the similar way; however, in present two degrees of free-dom for deep-groove ball bearing, the defect shapes have negligible effect as shown in Appendix A.

Fig. 3 shows the schematic diagram of bearing with surface defects. As the outer ring is fixed, the azimuth angle of outer raceway defect always keeps unchanged as:

$$\zeta_e^j = \alpha_e + (-1)^j W/D_e \ , j = 1,2 \tag{16}$$

where α_e is the azimuth angle of the outer race defect center. When multiple defects are distributed on the outer raceway, assuming the difference between the azimuth angle of nth defect and the azimuth angle of the first defect is θ_e^n, then the azimuth angle range of nth defect is

$$\zeta_e^{nj} = \zeta_e^j + \theta_e^n \ , j = 1,2. \tag{17}$$

The inner raceway defect moves with the inner ring at an angular velocity ω_i, the azimuth angle of the defect at the moment t can be expressed as

$$\zeta_i^j = \omega_i t + (-1)^j W/D_i \ , j = 1,2. \tag{18}$$

Similarly, when there are multiple defects on inner race, the azimuth angle range of the nth defect is

$$\zeta_i^{nj} = \zeta_i^j + \theta_i^n \ , j = 1,2. \tag{19}$$

The relative position between ball and defects can be judged from the azimuth angle of ball (Eq. (3)) and the azimuth angle range of surface defects (Eqs. (16)-(19)). β is used to represent the relative position between ball and the defect. $\beta = 1$ means the ball is right falling into the defect, and $\beta = 0$ means the ball is not in the defect which can be expressed as follows

$$\beta_i = \begin{cases} 1 & \zeta_i^1 \le \varphi_j \le \zeta_i^2, \ \text{ or } \zeta_i^{n1} \le \varphi_j \le \zeta_i^{n2} \\ 0 & \text{other cases} \end{cases} \tag{20}$$

$$\beta_e = \begin{cases} 1 & \zeta_e^1 \le \varphi_j \le \zeta_e^2, \ \text{ or } \zeta_e^{n1} \le \varphi_j \le \zeta_e^{n2} \\ 0 & \text{other cases} . \end{cases} \tag{21}$$

After considering the local defects, at the azimuth angle φ_j, the elastic deformation between ball and raceways will be changed from Eq. (4) to the following equation:

$$\delta_j = x\cos\varphi_j + y\sin\varphi_j - u - \beta_i\Delta_i - \beta_e\Delta_e \tag{22}$$

where Δ is the additional displacement of the ball center induced by a defect as given by Eq. (15).

Substituting Eq. (22) into Eq. (5), we can establish the motion differential equations of the bearing-rotor system considering the surface defects.

3. Numerical approaches

In present study, the fourth order Runge-Kutta method is used to solve the nonlinear differential equations (Eq. (14)). Eq. (14) can be written as

$$\dot{z}(t) = f(t, z(t)) . \tag{23}$$

Then, following the fourth order Runge-Kutta method,

$$z_{n+1} = z_n + \frac{h}{6}(K_1 + 2K_2 + 2K_3 + K_4) \tag{24}$$

where h is the step length in the program, $z_n = z(t_n)$ and

$$\begin{cases} K_1 = f(t_n, z_n) \\ K_2 = f(t_n + \dfrac{h}{2}, z_n + \dfrac{h}{2}K_1) \\ K_3 = f(t_n + \dfrac{h}{2}, z_n + \dfrac{h}{2}K_2) \\ K_4 = f(t_n + h, z_n + hK_3) . \end{cases} \tag{25}$$

The solving process is detailed as shown in Fig. 4.

4. Model validation

In order to verify the developed model, we compared the results from the present model with that in Ref. [9]. The same bearing, working conditions and defect parameters as in Ref. [9] were used.

When one single defect is located on the outer raceway, the

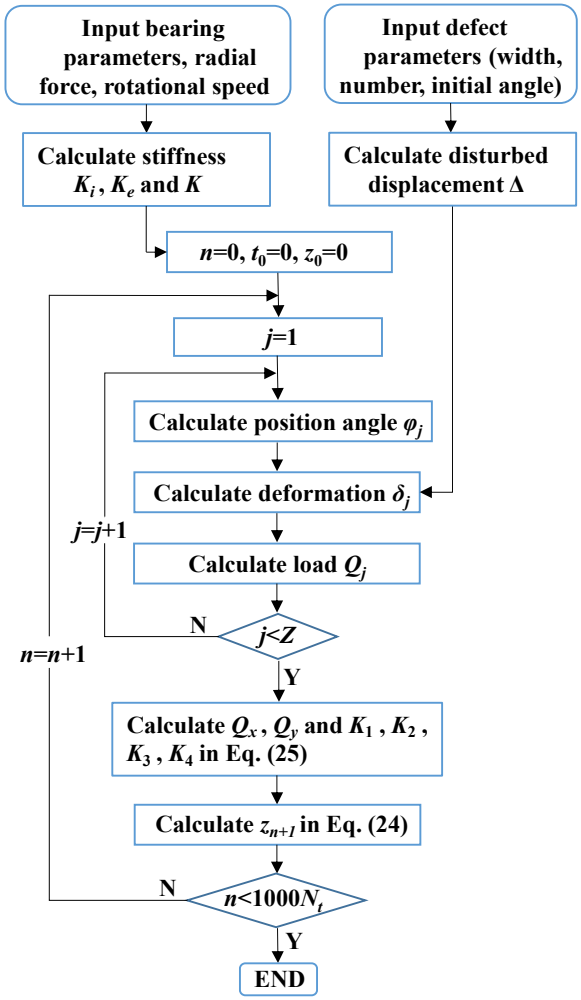

Fig. 4. The flowchart of the solving process.

numerical results calculated from our model are shown in Fig. 5 along with the results from Ref. [9], it can be found that the amplitude of the displacement and velocity is essentially the same, and the ball passing frequency on outer raceway (BPFO) f_{vc} is clearly visible in the spectrum. It is noted that, when solving the dynamic model, the initial displacement is assumed as zero, which may be far away from the real value; therefore, at the beginning of the solution process, the displacement will change and oscillate greatly and then gradually converge to the steady state solution. As the applied load is in vertical direction, thus the vibration in vertical direction is much severe, which is consistent with the experimental results.

Similarly, when a single defect is located on the inner raceway, the phase trajectories calculated from the present model are specially given in Fig. 6 to show the motion character at certain speed, which are almost the same as presented in the Ref. [9], and the slight differences in numerical results may be due to the different method of solving the differential equations of motion and not exactly same surface defect used, therefore the present model and numerical methods are verified.

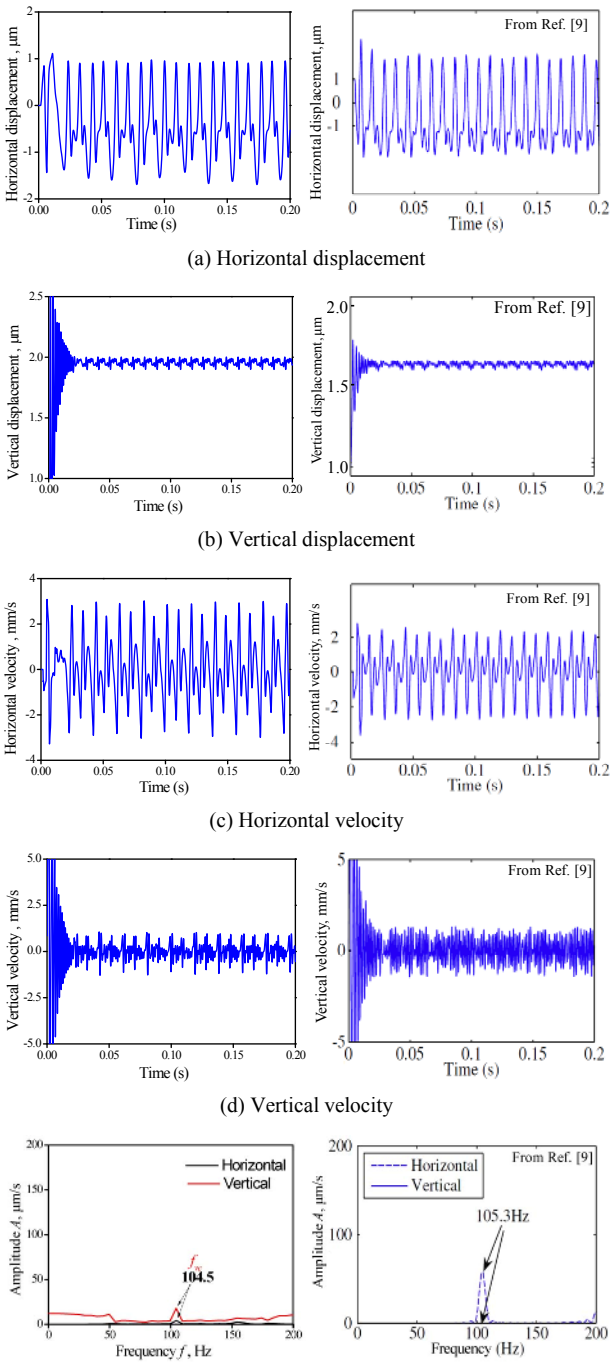

Fig. 5. The dynamic response and spectrum for a single defect on outer race.

5. Results and discussions

In following calculations, the initial values of the displacements and velocities in x and y directions are set as zero, namely, $z_1 = z_2 = z_3 = z_4 = 0$. The integration step length is chosen as 0.1 % of the exciting period, and totally N_t cycles are calculated. The results from the N_q^{th} cycle are extracted to represent the stable responses of the bearing-rotor system. In this section, SKF6002 deep groove ball bearing is used and its

Table 1. Parameters and working conditions of bearing SKF6002.

Inner race diameter d_i (mm)	9.369
Outer race diameter d_e (mm)	14.131
Ball number Z	9
Stiffness K (N/m$^{1.5}$)	7.055×10^9
Damping C (N·s/m)	200
Rotor mass M (kg)	0.6
Radial clearance u (μm)	20
Radial force F_r (N)	6.0
The calculate periods N_t	500
The result periods N_q	450

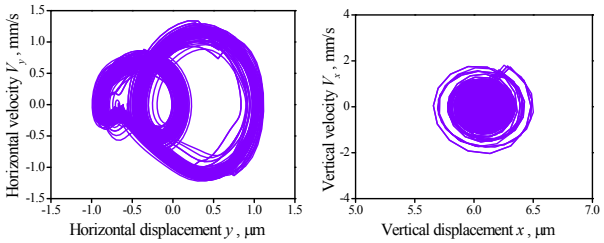

(a) Horizontal phase trajectories (b) Vertical phase trajectories

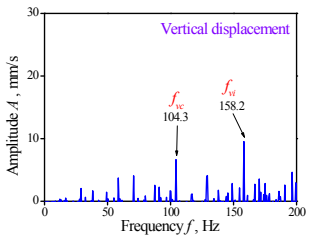

(c) Frequency spectrum for vertical velocity

Fig. 6. The phase trajectories and spectrum for a single defect on inner race.

parameters are shown in Table 1, where the stiffness coefficient K is obtained based on Eqs. (6)-(11) with the material properties, and the damping coefficient is from Ref. [9], which is commonly used in the similar studies.

In following study, we focus on the effect of defects on the bearing performance operated at high speed. Fig. 7 shows the bifurcation diagrams for the displacements and velocities of bearing center in x and y direction. Fig. 7(a) is for the case of a healthy bearing, while Fig. 7(b) is for the case of a bearing with a 2 mm wide defect on inner race. It can be observed that the motion of the bearing changes with increasing the rotational speed. As shown in Fig. 7(a), period-one motion can be found at rotational speed of 8000 rpm, and quickly changes into chaotic motion at the speed of 8200 rpm. Then period-ten, period-five and chaotic motion arise successively. Period-one motion emerges again at the speed of 11350 rpm. Comparing Fig. 7(b) with (a), the clear periodic motions almost disappear due to the presence of defect, and the region of chaos motion enlarges a lot. Besides, Fig. 8 shows the bifurcation diagrams for the case of a bearing with a 2 mm wide defect on outer race. The chaotic motion occurs in a wide rotational speed

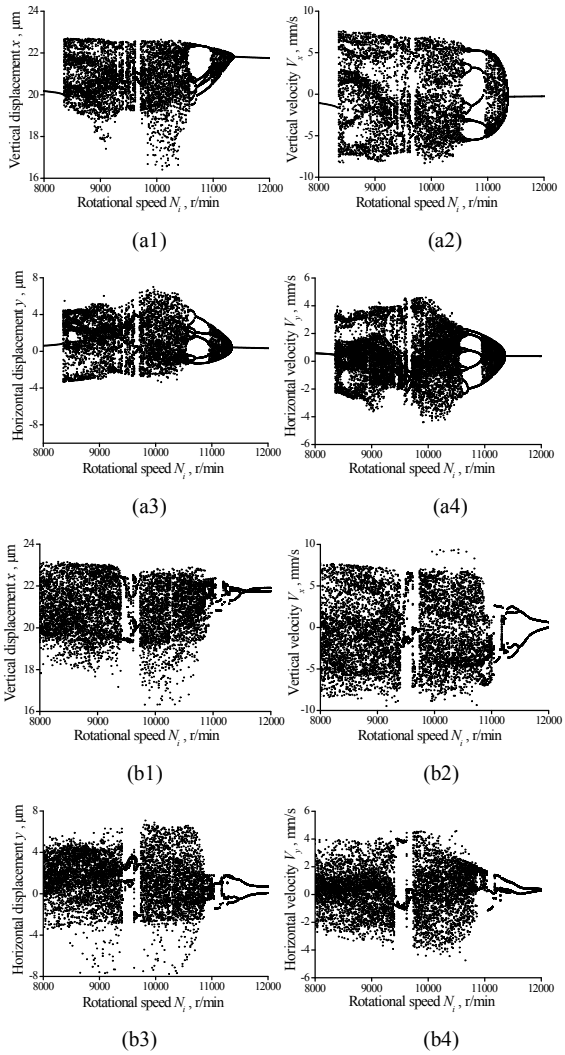

Fig. 7. The bifurcation diagrams of displacement and velocity in x and y direction: (a) Without defect (healthy); (b) with a defect on inner raceway.

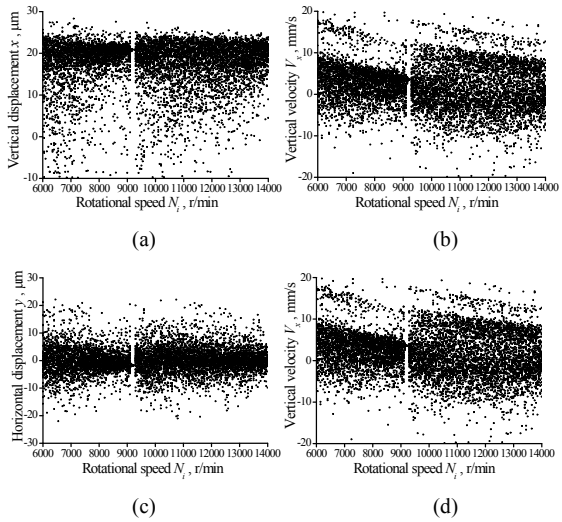

Fig. 8. The bifurcation diagrams of displacement and velocity in x and y direction (with a defect in outer raceway).

region from 6000 rpm to 14000 rpm which indicates that the defect on outer race has a much serious influence compared with defect on inner race, which will be further illustrated in the following sections. The bifurcation diagrams for the bearing with 0.5 mm, 1 mm and 2 mm defects are also obtained, but not shown due the space limit. It is found that, with the increase of the defect size, the chaotic motion gradually extends to both low and high speed regions and the detailed routine to chaos represents slight difference. Despite of these, on the whole, the defects with different sizes have similar effect on the dynamic behaviors of system as the case with 2 mm defect.

Table 2. Characteristic frequencies of the bearing (at the speed of 12000 rpm).

BPFO f_{vc} (Hz)	717.71
BPFI f_{vi} (Hz)	1082.30
Cage frequency f_c (Hz)	79.74
Shaft frequency f_i (Hz)	200

Next, the case for the rotational speed of 12000 rpm is investigated in detail. Table 2 gives the characteristic frequencies of the bearing at this speed.

5.1 Effect of the defect size

In the manufacturing and service process, the defect appeared on raceways or ball surface may be random in size. In this section, the effect of the defect size on the bearing behav-

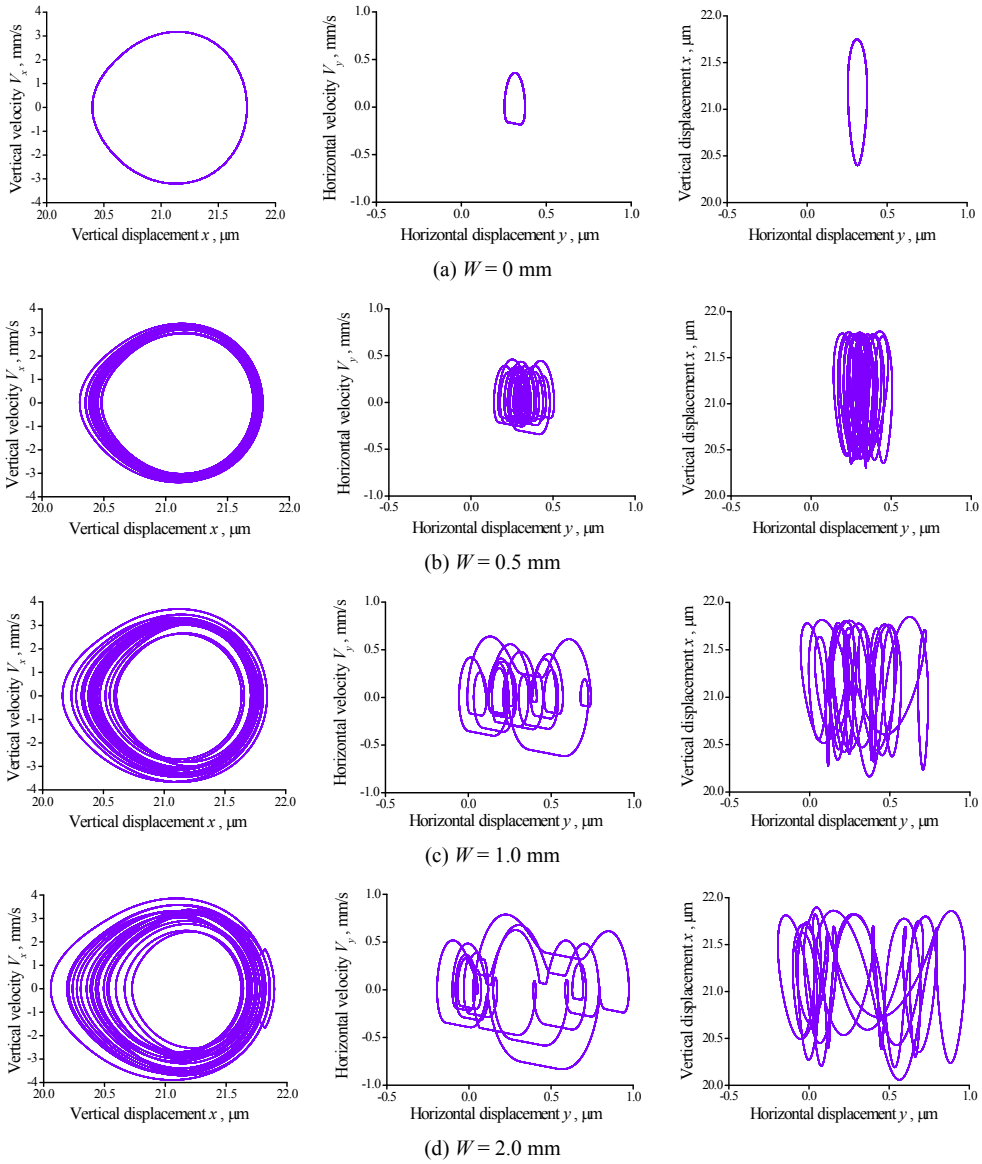

(a) W = 0 mm

(b) W = 0.5 mm

(c) W = 1.0 mm

(d) W = 2.0 mm

Fig. 9. The phase trajectories, and shaft center orbits for a single defect on inner raceway: (a) W = 0 mm (healthy bearing); (b) W = 0.5 mm; (c) W = 1.0 mm; (d) W = 2.0 mm.

ior is investigated. Fig. 9 shows the phase trajectories and shaft center orbits for the inner raceway defect with width of 0 mm, 0.5 mm, 1.0 mm and 2.0 mm. It is obviously shown in Fig. 9, with the increase of the defect size, the phase trajectories and shaft center orbits become more complicated. It implies that the bearing vibration will be strengthened, and therefore reduce the precision of bearing operation. According to Fig. 9(a), both the phase trajectories and shaft center orbit of a healthy bearing indicate period-one motion. However, when the defect appears on inner raceway, the motion is no longer periodic as shown in Figs. 9(b)-(d), and with the increase of the defect size, the bearing vibration obviously increases. Fig. 10 shows the spectrums of vertical displacements for different size of inner raceway defect. The vibrations only occur at f_{vc} and its multipliers when the bearing is in healthy condition. However, f_i, f_c and other frequencies appear when a defect arises on inner race; and the amplitudes of spectrums turn to be higher with the larger defect.

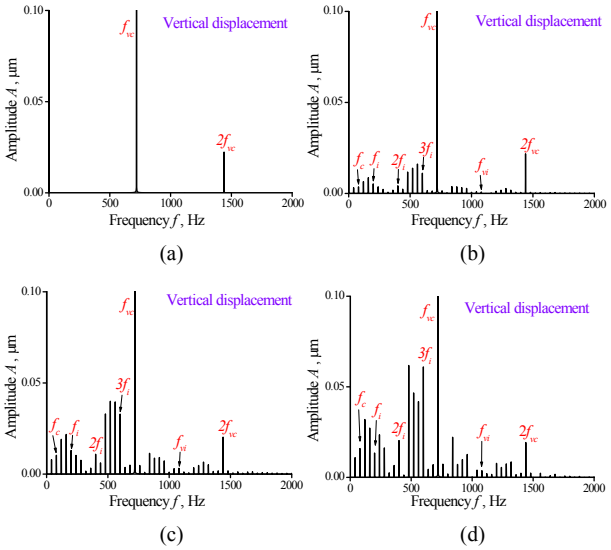

Fig. 10. The spectrums of vertical displacements for a single defect on inner raceway: (a) W = 0 mm (healthy bearing); (b) W = 0.5 mm; (c) W = 1.0 mm; (d) W = 2.0 mm.

5.2 Effect of the defect number

Besides the defect size, the number of defects is also random in a real bearing. It is desirable to explore the influence of multiple defects on bearing performance, which will provide theoretical support for bearing default diagnoses. As shown in Fig. 11, the phase trajectories and shaft center orbits become

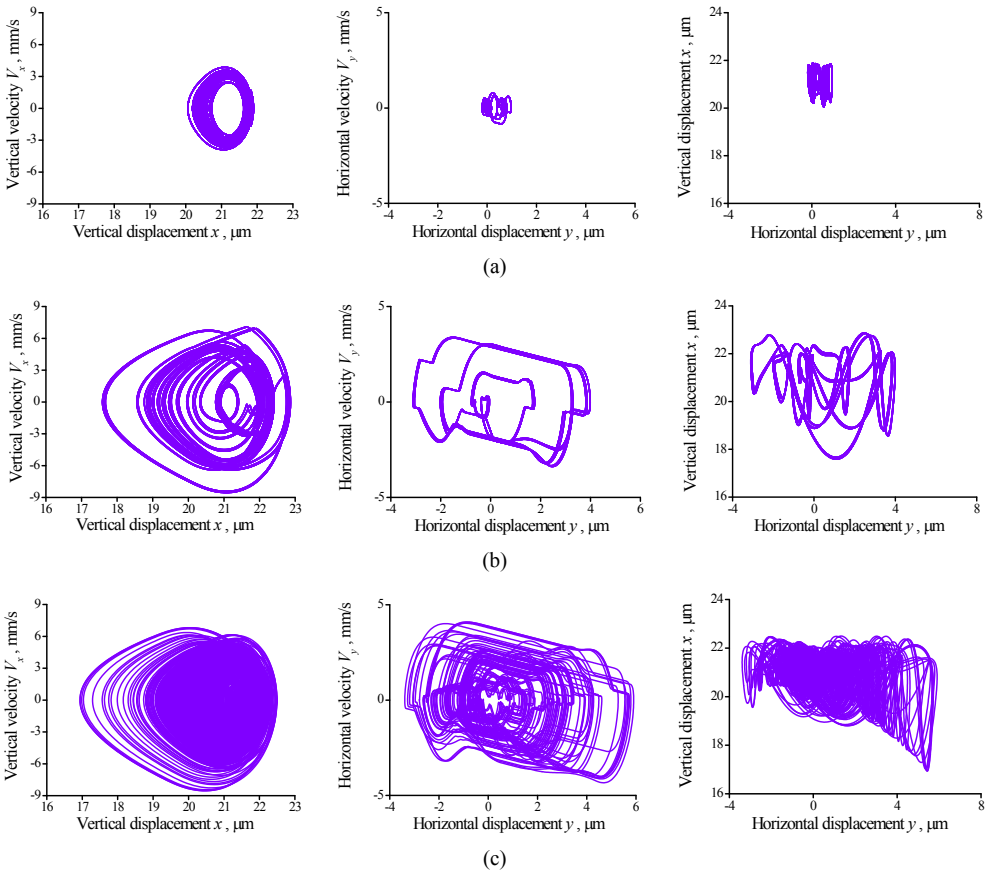

Fig. 11. The phase trajectories and shaft center orbits for different number of defects on inner raceway: (a) One defect; (b) two defects; (c) three defects.

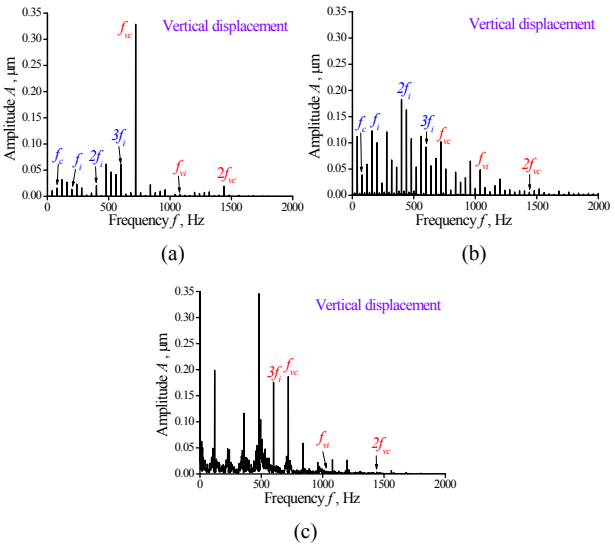

Fig. 12. The spectrums of vertical displacements for different number of defects on inner raceway: (a) One defect; (b) two defects; (c) three defects.

more complex and have a wider range with the increase in the number of defects, which indicates the vibration has been strengthened with the increase in the number of defects. Similarly, as shown in Fig. 12, the spectrums turn to be more complicated and the amplitudes become higher as the defect number increases.

5.3 Effect of the defect location

5.3.1 Defect on different races

Generally speaking, defects may appear on both the inner raceway and outer raceway, it is necessary to explore the effect of defect on different races. As observed in Fig. 13, the bearing-rotor system is in periodic motion when defect does not exist, the vibrations only occur at f_{vc} and its multipliers. However, the phase trajectories and shaft center orbits become complicated and the periodic motion has been ruined when the defect is presented on raceways. It is obvious that the outer raceway defect has greater influence on the vibration comparing with the inner raceway defect, as the outer raceway defect is always located in the loaded zone, while the inner raceway defect rotates with the inner ring which will alleviate the influence of defect on vibration. When the defect located on outer raceway, in addition to f_{vc} and its multipliers, there are also f_i, f_c and other low frequencies in the spectrum. For the case of inner raceway defect, the vibration at low frequencies turn to be clear and f_{vi} appears in the spectrum, and the spectrum amplitudes of inner race are lower than outer race, which can be used as a basis for monitoring the operation condition of the bearing in project.

5.3.2 Defect at different locations on the same race

During service process, the defect on inner raceway will rotate with inner ring, therefore its position will have no effect on bearing dynamic behavior; while the defect on outer raceway is different as the outer ring usually is fixed in application.

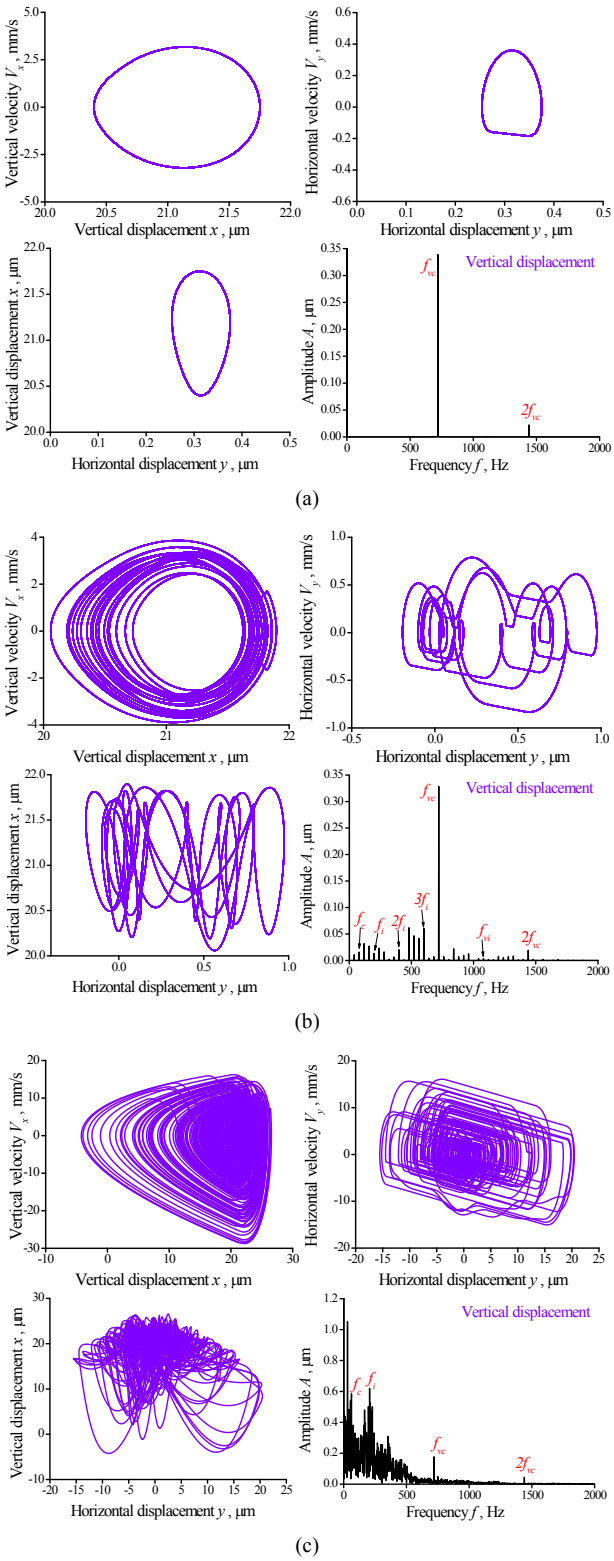

Fig. 13. The phase trajectories, shaft center orbits, and spectrums for defect on different races: (a) Healthy bearing; (b) single defect on inner race; (c) single defect on outer race.

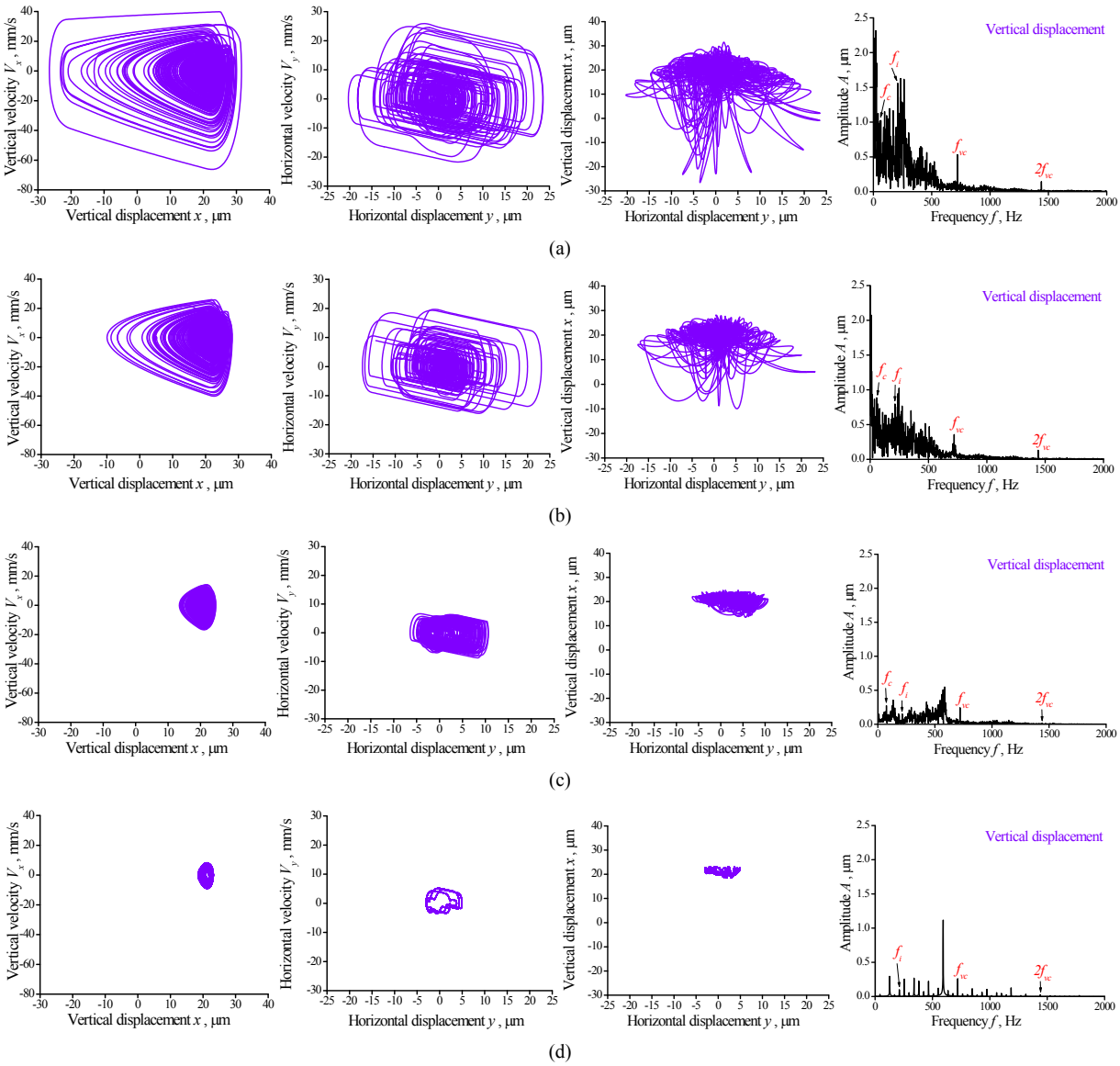

Fig. 14. The phase trajectories, shaft center orbits and spectrums for a single defect on different location of outer race: (a) 0 degrees; (b) 10 degrees; (c) 30 degrees; (d) 90 degrees.

he outer raceway defects mostly appear in the loaded region; based on the developed model, we investigate the effect of the outer raceway defect position. Fig. 14 shows the phase trajectories, shaft center orbits, and the spectrums for vertical displacements of bearing with single defect located on different azimuth angle of outer raceway. It is obvious that the range of phase trajectory and shaft center orbit become small, and the amplitudes of spectrums for vertical displacements become low and simple as the defect moves away from the loaded zone. Therefore, a conclusion can be drawn from Fig. 14 that, outer raceway defect located in the loaded zone causes remarkable vibration, and the vibration will be gradually weakened with the defect away from the loaded zone. As for the spectrums, the characteristic frequencies are almost the same, but the spectrum amplitudes become smaller with the defect away from the loaded zone.

5.4 Effect of the defect distribution

Multiple defects may arise on raceways in the manufacturing and service process, and the defect distribution may be uniform or random, which will induce different dynamic behavior and vibration. In this section, three defects are assumed to discuss the effect of the defect distribution. Uniform distribution of defects means that the three defects are 120 degrees apart from each other; while random distribution of defects means that the defects may appear any positions randomly.

The shaft center orbits for different distributions of defects on inner race are shown in Fig. 15, and the defect width is set as 0.5 mm, 1.0 mm and 2.0 mm, respectively. It can be seen that when the defects are uniformly distributed, the bearing vibration increases obviously with the defect size increasing. However, random distribution of defects results in different

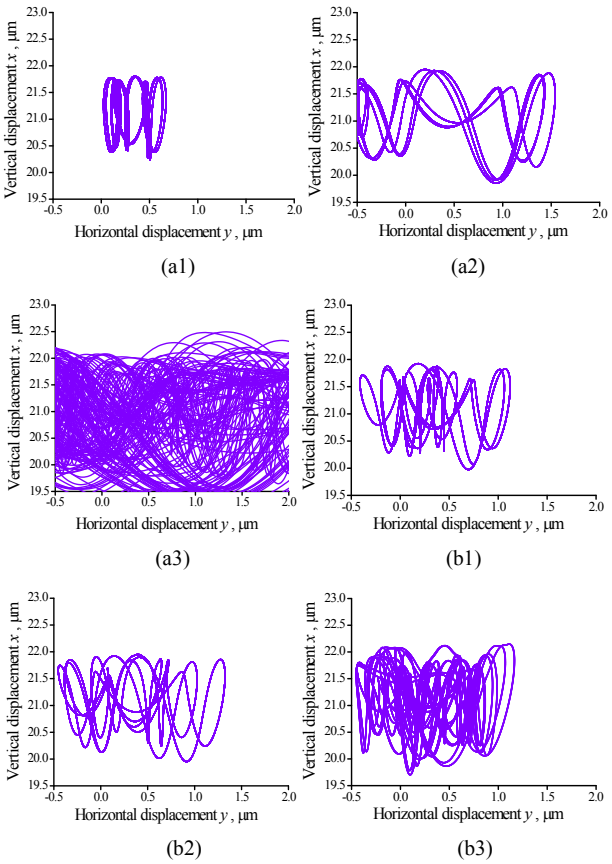

Fig. 15. The shaft center orbits for defects on inner race: (a) At a uniform distribution; (b) at a random distribution; (a1) (b1) 0.5 mm; (a2) (b2) 1.0 mm; (a3) (b3) 2.0 mm.

behaviors as shown in Fig. 15(b). When the defects are randomly distributed, the shaft center orbits become relatively complicated with the increase of defect size, but the range of displacement fluctuation in the horizontal and vertical directions is almost unchanged. Therefore, it can be found that the random distribution of defects has a certain inhibition to the vibration caused by the increase of the defect size relative to the uniform distribution. That is because the SKF6002 bearing has nine balls, when three defects are uniformly distributed, there are three balls fall into the defects at the same time, which will cause resonance and the vibration of the bearing will be enlarged. On the contrast, for the case of random distribution, generally it is impossible to appear the above situation which has inhibitory effects on the vibration of bearing relative to the uniform distribution of defects. In Fig. 16, there are high-amplitude frequencies occurring almost periodically when defects are uniformly distributed, but the spectrum becomes irregular for the random distribution of defects. It also indicates that periodic vibration occurs when defects are uniformly distributed.

The shaft center orbit for different distributions of defects on outer raceway is shown in Fig. 17. Comparing with Fig. 15, the distribution of outer raceway defects almost has no effect on the vibration caused by the increase of the defect size. As

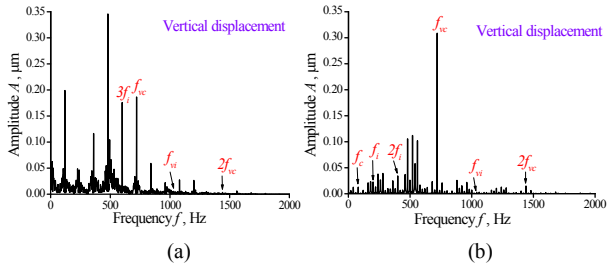

Fig. 16. The spectrums of vertical displacements for defects on inner race: (a) At a uniform distribution; (b) at a random distribution.

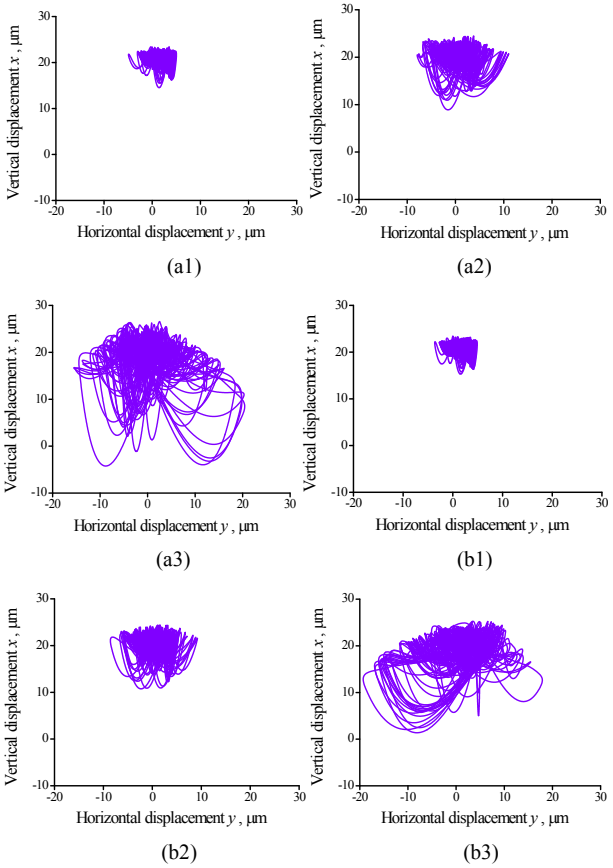

Fig. 17. The shaft center orbits for defects on outer race: (a) At a uniform distribution; (b) at a random distribution; (a1) (b1) 0.5 mm; (a2) (b2) 1.0 mm; (a3) (b3) 2.0 mm.

the outer raceway is fixed, only the defect in load zone takes effect, while the distribution of defects has a tiny effect. Fig. 18 shows that, the spectrums of two kinds of distributions of defects on outer raceway are almost the same, which also indicates the distribution of defects on outer raceway has a negligible effect on vibration.

5.5 Effect of the defects coupled with interface friction

In previous sections, the effect of defects is investigated with no friction force considered between ball and races. This section will focus on the effect of defects with consideration

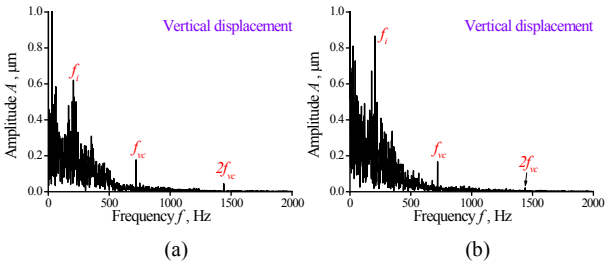

Fig. 18. The spectrums of vertical displacements for defects on outer race: (a) At a uniform distribution; (b) at a random distribution.

of friction force between ball and races. The friction coefficient between ball and raceways is approximately set as 0, 0.007 and 0.07. The tangential stress at any point in the contact zone can be evaluated by assuming Hertz pressure distribution:

$$\tau = \mu \frac{3Q}{2\pi ab}\sqrt{1-(\frac{x}{a})^2-(\frac{y}{b})^2} \tag{26}$$

where Q is the normal contact force between ball and raceways which is calculated by Eq. (5), a and b are the semi-major axes of the Hertz contact elliptical region.

The effect of defects coupled with interface friction is shown in Fig. 19. The vibration of the bearing is strengthened after considering the tangential friction between ball and races whether the defects are on inner race or outer race. Because the friction hinders the motion of balls, making the forces on the balls more complicated which leads to the increase of uncertainty of the motion and the enhancement of the vibration. Moreover, the value of friction coefficient has greater impact on the vibration for the defects on inner race compared with outer race as ball pass frequency on inner race is greater than that of outer race.

5.6 Effect of the defects coupled with eccentricity of bearing-rotor system

In practical application, the eccentricity of bearing-rotor system may exist due to manufacturing and/or installation error. The defect coupled with eccentricity may cause increasing noise and serious vibration, it is necessary to explore the effect of defect with consideration of eccentricity of bearing-rotor system.

Three eccentricities of 1, 3, 5 μm are considered and the results are shown in Figs. 20 and 21 for inner and outer raceways, respectively. It can be found that the eccentricity makes the shaft center orbits more complicated, the vibration range of shaft center increases obviously. A greater increase of vibration arises when the eccentricity has a small scale increase, which means that the eccentricity has a great influence on the bearing vibration. In addition, the eccentricity has a larger effect for the case of defects on inner raceway. With the increase of eccentricity, the vibration induced by inner raceway defects becomes larger than that induced by outer raceway

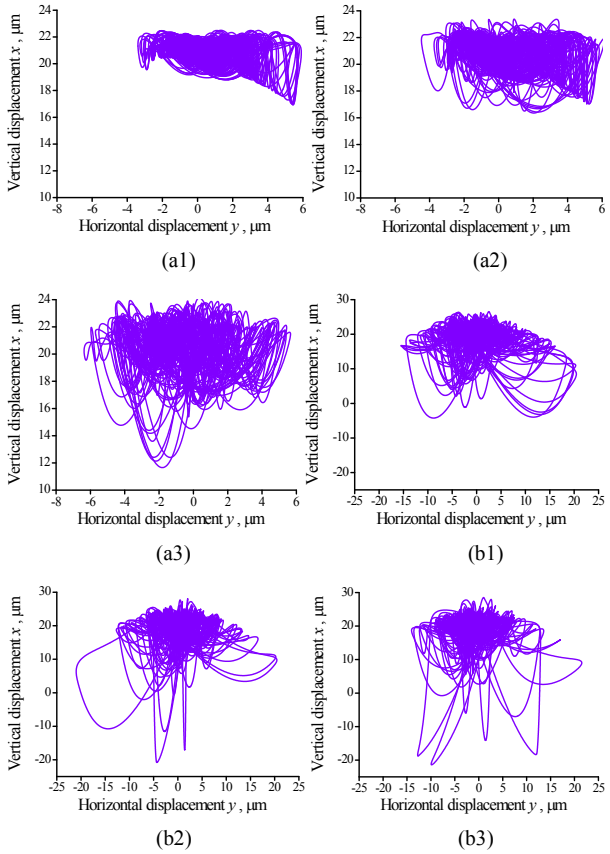

Fig. 19. The shaft center orbits for defects coupled interface friction: (a) Inner raceway; (b) outer raceway; (a1) (b1) μ = 0; (a2) (b2) μ = 0.007; (a3) (b3) μ = 0.07.

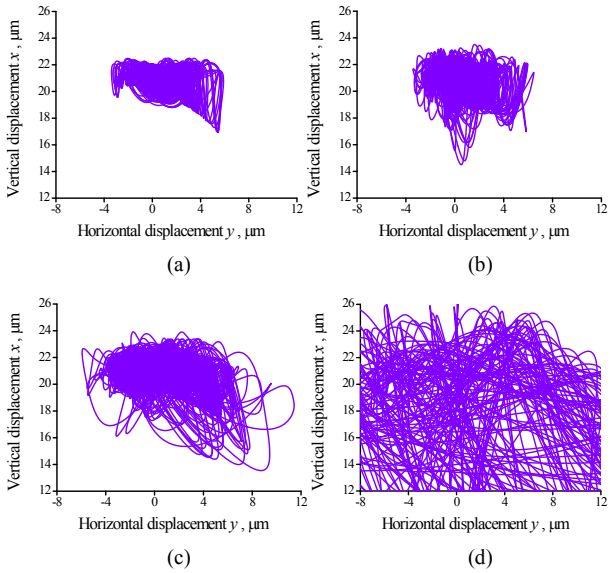

Fig. 20. The shaft center orbits for defects on inner race coupled eccentricity: (a) e = 0; (b) e = 1 μm; (c) e = 3 μm; (d) e = 5 μm.

defects as the outer ring is fixed, while the inner ring rotates with the shaft.

In all, this paper studies the effects of the defect size, num-

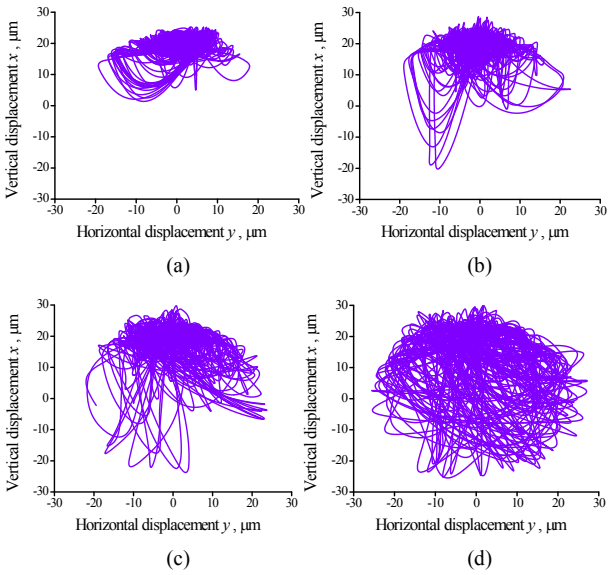

Fig. 21. The shaft center orbits for defects on outer raceway coupled eccentricity: (a) e = 0; (b) e = 1 μm; (c) e = 3 μm; (d) e = 5 μm.

ber, location, distribution and the coupled effects with friction coefficient and eccentricity. Some new findings are explored, which will help to understand the effect of various defects on the bearing behaviors as follows: (1) The randomly distributed defects may suppress the vibration caused by the increase of the defect size relative to the uniform distribution; (2) the vibration of the bearing is strengthened after considering the tangential friction between ball and races whether the defects are on inner race or outer race; (3) with the increase of eccentricity, the vibration induced by inner raceway defects becomes larger than that induced by outer raceway defects as the outer ring is fixed, while the inner ring rotates with the shaft.

6. Conclusions

A dynamic model is developed to investigate the effect of defects on races on the nonlinear dynamic behaviors of rolling bearing. The following conclusions can be drawn based on systematic analysis:

(1) Despite of the defect size, the practical randomly distributed defects will inhibit the induced vibration, comparing with ideally evenly distributed defects.

(2) The vibration of the bearing is aggravated when considering the tangential friction force, and when the defects on inner raceway, the influence of the variation of friction coefficient on the bearing vibration is obviously higher than that of the outer raceway.

(3) The effect of eccentricity of the bearing-rotor on the bearing vibration may exceed that from the race defects, and become overwhelming with the increase of eccentricity, and the amplitude of the vibration for the case of inner raceway defect is larger than that for the outer raceway defect.

(4) For healthy bearing, the vibration only occurs at f_{vc} and its multipliers, while the defects on raceway will induce extra vibration at certain characteristic frequencies. The outer race defect will produce characteristic frequencies f_i, f_c and other low frequencies in the spectrum besides f_{vc} and its multipliers; while the inner raceway defect induces characteristic frequency f_{vi}, and the spectrum amplitudes are lower than outer raceway. In addition, the spectrum turns to be more complex when there are multiple defects. These characteristic frequencies induced by the raceway defects can be used as a basis for status monitoring of machine systems.

(5) By comparing the measured signals with the characteristics of the phase trajectories, shaft center orbits and spectrums obtained from the model, the defect types may be recognized.

Acknowledgments

This work was supported by the National Natural Science Foundation of China (Project no. 51405017, U1637205).

Nomenclature

a, b : Long and short axis of the ellipse in Hertz contact region
C : Damping coefficient
d : Displacement of inner race groove bottom
d_i, d_e : Inner race and outer race diameter of bearing
D : Diameter of the ball
D_i : Inner race diameter of groove bottom
D_e : Outer race diameter of groove bottom
e : Eccentricity of the bearing-rotor system
E' : Integrated elastic modulus
E_1,E_2 : Integrated elastic modulus
f_c : Cage frequency
f_i : Shaft frequency
f_{vc} : Ball pass frequency of outer race
f_{vi} : Ball pass frequency of inner race
F_r : Radial force
K : Stiffness
K_i,K_e : Stiffness of the ball in contact with inner and outer raceway
$L_1(\kappa)$, $L_2(\kappa)$: First and second complete elliptic integral
M : Rotor mass
N_i : Rotational speed
N_q : The result periods
N_t : The calculated periods
Q : Contact load
t : Time
u : Radial clearance of bearing
W : Width of the defect
x : Vertical displacement of inner ring center
y : Horizontal displacement of inner ring center
Z : Number of balls
ω_c : Orbital angular velocity of a ball
ω_i : Inner ring angular velocity
φ_j : Azimuth angle of the jth ball
δ : Elastic deformation
ρ_i, ρ_e : Inner and outer race curvature of groove bottom

ν_1, ν_2 : Poisson's ratio of two contact bodies
κ : Contact ellipticity
Δ : Addition displacement of ball center induced by a defect
α_e : Initial azimuth angle of the outer race defect center
θ_i, θ_e : Angle between other defect and the first defect on inner race and outer race
ζ_i^1, ζ_i^2 : Azimuth angle range of inner race defect
ζ_e^1, ζ_e^2 : Azimuth angle range of outer race defect
μ : Friction coefficient between ball and raceways
τ : Tangential stress at any point in the contact zone

References

[1] N. Tandon and A. Choudhury, A review of vibration and acoustic measurement methods for the detection of defects in rolling element bearings, *Tribology International*, 32 (8) (1999) 469-480.

[2] P. D. McFadden and J. D. Smith, Model for the vibration produced by a single point defect in a rolling element bearing, *Journal of Sound and Vibration*, 96 (1) (1984) 69-82.

[3] P. D. McFadden and J. D. Smith, The vibration produced by multiple point defects in a rolling element bearing, *Journal of Sound and Vibration*, 98 (2) (1985) 263-273.

[4] N. Tandon and A. Choudhury, An analytical model for the prediction of the vibration response of rolling element bearings due to a localized defect, *Journal of Sound and Vibration*, 205 (3) (1997) 275-292.

[5] J. Sopanen and A. Mikkola, Dynamic model of a deep-groove ball bearing including localized and distributed defects. Part 1: Theory, *Proceedings of the Institution of Mechanical Engineers, Part K*: *Journal of Multi-body Dynamics*, 217 (3) (2003) 201-211.

[6] J. Sopanen and A. Mikkola, Dynamic model of a deep-groove ball bearing including localized and distributed defects. Part 2: Implementation and results, *Proceedings of the Institution of Mechanical Engineers, Part K*: *Journal of Multibody Dynamic*, 217 (3) (2003) 213-223.

[7] Z. Kiral and H. Karagülle, Vibration analysis of rolling element bearings with various defects under the action of an unbalanced force, *Mechanical Systems and Signal Processing*, 20 (8) (2006) 1967-1991.

[8] A. Ashtekar, F. Sadeghi and L. E. Stacke, A new approach to modeling surface defects in bearing dynamics simulations, *Journal of Tribology*, 130 (4) (2008) 041103-1-041103-8.

[9] A. Rafsanjani, S. Abbasion, A. Farshidianfar and H. Moeenfard, Nonlinear dynamic modeling of surface defects in rolling element bearing systems, *Journal of Sound and Vibration*, 319 (3-5) (2009) 1150-1174.

[10] M. S. Patil, J. Mathew, P. K. Rajendrakumar and S. Desai, A theoretical model to predict the effect of localized defect on vibrations associated with ball bearing, *International Journal of Mechanical Sciences*, 52 (9) (2010) 1193-1201.

[11] M. Nakhaeinejad and M. D. Bryant, Dynamic modeling of rolling element bearings with surface contact defects using bond graphs, *Journal of Tribology*, 133 (1) (2011) Article ID 011102.

[12] P. G. Kulkarni and A. D. Sahasrabudhe, A dynamic model of ball bearing for simulating localized defects on outer race using cubic hermite spline, *Journal of Mechanical Science and Technology*, 28 (9) (2014) 3433-3442.

[13] T. Govardhan, A. Choudhury and D. Paliwal, An investigation into defect induced excitations in rolling element bearings under dynamic radial load, *2015 International Conference on Industrial Instrumentation and Control (ICIC)*, Pune, India (2015) 217-222.

[14] J. Liu, Y. Shao and W. D. Zhu, A new model for the relationship between vibration characteristics caused by the time-varying contact stiffness of a deep groove ball bearing and defect sizes, *Journal of Tribology*, 137 (3) (2015) Article ID 031101.

[15] S. Sassi, B. Badri and M. Thomas, A numerical model to predict damaged bearing vibrations, *Journal of Vibration and Control*, 13 (11) (2007) 1603-1628.

[16] H. Arslan and N. Aktürk, An investigation of rolling element vibrations caused by local defects, *Journal of Tribology-Transactions of the ASME*, 130 (4) (2008) Article ID 041101.

[17] V. N. Patel, N. Tandon and R. K. Pandey, A dynamic model for vibration studies of deep groove ball bearings considering single and multiple defects in races, *Journal of Tribology*, 132 (4) (2010) Article ID 041101.

[18] W. Wang et al., Effect of the inhomogeneity in races on the dynamic behavior of rolling bearing, *Journal of Vibration & Acoustics*, 137 (6) (2015) Article ID 061015.

[19] F. P. Wardle, Vibration forces produced by waviness of the rolling surfaces of thrust loaded ball bearings Part 1: Theory, *Proceedings of the Institution of Mechanical Engineers Part C*: *Journal of Mechanical Engineering Science*, 202 (5) (1988) 305-312.

[20] N. Aktürk, The effect of waviness on vibrations associated with ball bearings, *Journal of Tribology*, 121 (4) (1999) 667-677.

[21] N. Lynagh, H. Rahnejat, M. Ebrahimi and R. Aini, Bearing induced vibration in precision high speed routing spindles, *International Journal of Machine Tools and Manufacture*, 40 (4) (2000) 561-577.

[22] S. P. Harsha, K. Sandeep and R. Prakash, Non-linear dynamic behaviors of rolling element bearings due to surface waviness, *Journal of Sound and Vibration*, 272 (3-5) (2004) 557-580.

[23] M. Tiwari, K. Gupta and O. Prakash, Effect of radial internal clearance of a ball bearing on the dynamics of a balanced horizontal rotor, *Journal of Sound and Vibration*, 238 (5) (2000) 723-756.

Appendix

A. Effect of defect shape

The effect of different defect shapes including triangular, parabolic and rectangular forms as shown in Fig. A.1 is inves-

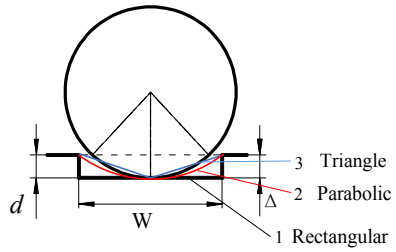

Fig. A.1. Schematic diagram for different defect shape.

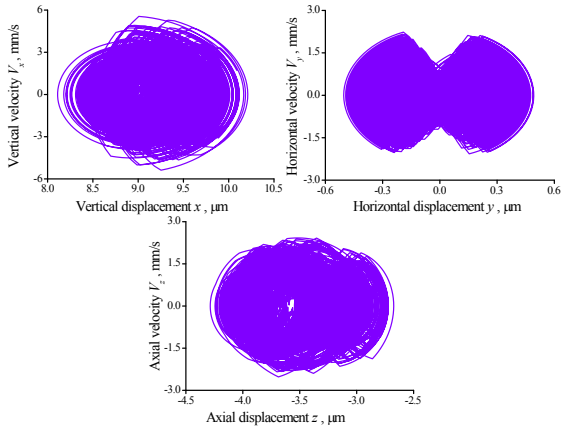

(a) Defect with rectangular cross-section

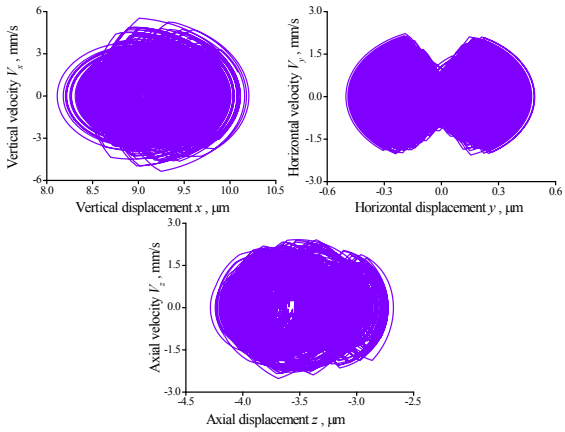

(b) Defect with parabolic cross-section

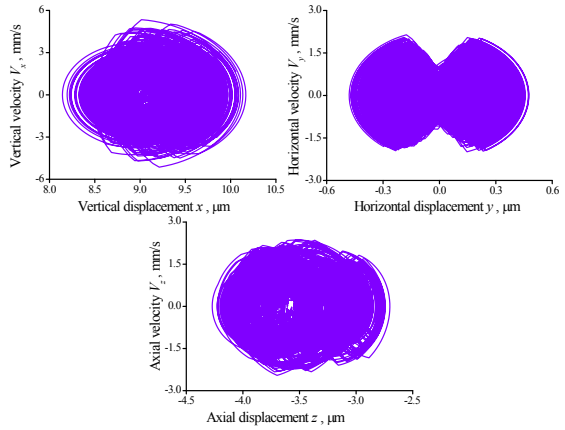

(c) Defect with triangular cross-section

Fig. A.2. The effect of the defect shape (W = 2.0 mm).

tigated. The results are presented in Fig. A.2. It can be found that the defects with different shapes hardly influence the dynamic behaviors of the investigated bearing; the reason is that the established dynamic model for the deep groove ball bearing has two degrees of freedom, and the defect depth is much small comparing with bearing elements; consequently, when the balls roll over the defect, the change of contact deformation is negligibly small. Therefore, only rectangular defect is presented in this paper.

Ziqang Zhao received his Ph.D. degrees in mechanical engineering from Beijing Institute of Technology (BIT), China, in 2009. He is an Associate Professor in BIT. His research areas cover dynamic theory and experiment of gear transmission system and rolling bearing, numerical simulation of lubrication and mechanical design.

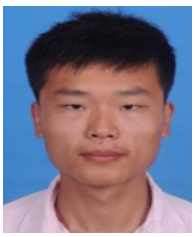

Xuebin Yin received his master degree from Beijing Institute of Technology (BIT), China in 2018. His current research interests include dynamic theory and experiment of rolling bearing.

Wenzhong Wang received his Ph.D. degree in mechanical engineering from Tsinghua University, China, in 2003. He joined School of Mechanical Engineering at Beijing Institute of Technology from 2006. His current position is a Professor and Director of Department of Machine Design. His research areas cover modeling of lubricated contact problem, contact model for inhomogeneous and function gradient materials, dynamics of rolling bearing, thermal analysis.